DOI: 10.1021/ic901531e

Inorganic Chemistry
Article

Synthesis, Structure, and Two-Photon Absorption Studies of a Phosphorus-Based Tris Hydrazone Ligand (*S*)P[N(Me)N=CH-C_6H_3-*2*-OH-*4*-N(CH_2CH_3)$_2$]$_3$ and Its Metal Complexes

Vadapalli Chandrasekhar,* Ramachandran Azhakar, Balasubramanian Murugesapandian, Tapas Senapati, Prasenjit Bag, Mrituanjay D. Pandey, Sandeep Kumar Maurya, and Debabrata Goswami*

Department of Chemistry, Indian Institute of Technology Kanpur, Kanpur-208016, India

Received August 2, 2009

A phosphorus-supported multidentate ligand (*S*)P[N(Me)N=CH-C_6H_3-*2*-OH-*4*-N(CH_2CH_3)$_2$]$_3$ (**1**) has been used to prepare mononuclear complexes LM [M=Fe (**2**) Co (**3**)] and trinuclear complexes L_2M_3 [M=Mn (**4**), Ni (**5**), Zn (**6**), Mg (**7**), Cd (**8**)]. In both **2** and **3** the ligand binds the metal ion in a facial coordination mode utilizing three imino nitrogen (3N) and three phenolic oxygen (3O) atoms. The molecular structures of L_2Mn_3, L_2Ni_3, L_2Zn_3, L_2Mg_3, and L_2Cd_3 (**4**−**8**) are similar; two trihydrazone ligands are involved in coordination to hold the three metal ions in a linear fashion. Each of the trishydrazone ligands behaves as a trianionic hexadentate ligand providing three imino and three phenolic oxygen atoms for coordination to the metal ions. The coordination environment around the two terminal metal ions is similar (3N, 3O) while the central metal ion has a 6O coordination environment. Third-order non-linear optical properties of these compounds as measured by their two-photon absorption (TPA) cross section reveals that while **1** does not possess obvious TPA activity, complexes **2** (3213 GM) and **4** (3516 GM) possess a large TPA cross section at 770 nm.

Introduction

Molecules with large two-photon absorption (TPA) cross sections are extensively explored for applications in the two-photon dynamic therapy,[1] optical power limiting materials,[2] three-dimensional (3-D) storage media,[3] up-converted lasing,[4] microfabrication,[5] and so forth. The efficiency of a two-photon process requires materials with large two-photon absorption cross sections (TPACS), which are directly related to the imaginary part of the third order non-linear susceptibility.[6] Since the electron delocalization plays an important role in TPA activity, the extension of electron delocalization has been an important feature in designing molecules with enhanced third-order optical non-linearity.[7]

Most of the research on molecules possessing TPA activity has been focused on organic dyes based on heteroaromatics,[8] and/or dendritic systems containing triphenylamine[9] and anthracene[10] derivatives. In all of these systems electron-releasing and -withdrawing groups are appropriately placed in the molecule and are bridged by a π-conjugated manifold. In addition to this well-established strategy, in the recent

*To whom correspondence should be addressed. E-mail: vc@iitk.ac.in (V.C.), dgoswami@iitk.ac.in (D.G.).

(1) (a) Bhawalkar, J. D.; Kumar, N. D.; Zhao, C. F.; Prasad, P. N.; Clin, J. *Laser Med. Surg*. **1997**, *15*, 201. (b) Brott, L. L.; Naik, R. R.; Pikas, D. J. *Nature* **2001**, *413*, 291.

(2) (a) He, G. S.; Bhawalkar, J. D.; Zhao, C. F.; Prasad, P. N. *Appl. Phys. Lett*. **1995**, *67*, 2433. (b) Ehrlich, J. E.; Wu, X. L.; Lee, I.-Y. S.; Hu, Z.-Y.; Röckel, H.; Marder, S. R.; Perry, J. W. *Opt. Lett*. **1997**, *22*, 1843. (c) Baldeck, P. L.; Morel, Y.; Andraud, C.; Nicoud, J. F.; Ibanez, A. *Photonics Sci. News* **1999**, *4*, 5. (d) Brixner, T.; Damrauer, N. H.; Niklaus, P.; Gerber, G. *Nature* **2001**, *414*, 57. (e) Perry, J. W.; Hales, J. M.; Chi, S.-H.; Cho, J.-Y.; Odom, S.; Zhang, Q.; Zheng, S.; Schrock, R. R.; Screen, T. E. O.; Anderson, H. L.; Barlow, S.; Marder, S. R. *Polym. Prepr*. **2008**, *49*, 989–990. (f) Belfield, K. D.; Bondar, M. V.; Hernandez, F. E.; Przhonska, O. V. *J. Phys. Chem. C* **2008**, *112*, 5618–5622. (g) Qian, Y.; Meng, K.; Lu, C.-G.; Lin, B.; Huang, W.; Cui, Y.-P. *Dyes Pigm*. **2009**, *80*, 174–180.

(3) (a) Day, D.; Gu, M.; Smallridge, A. *Opt. Lett*. **1999**, *24*, 948. (b) Zhou, W. H.; Kuebler, S. M.; Braun, K. L. *Science* **2002**, *296*, 1106.

(4) (a) Abbotto, A.; Beverina, L.; Bozio, R.; Bradamante, S.; Pagani, G. A.; Signorini, R. *Synth. Met*. **2001**, *121*, 1755. (b) Abbotto, A.; Beverina, L.; Bozio, R.; Bradamante, S.; Ferrante, C.; Pagani, G. A.; Signorini, R. *Adv. Mater*. **2000**, *12*, 1963.

(5) (a) Cumpston, B. H.; Ananthavel, S. P.; Barlow, S.; Dyer, D. L.; Ehrlich, J. E.; Erskine, L. L.; Heikal, A. A.; Kuebler, S. M.; Lee, I. Y. S.; McCord-Maughon, D.; Qin, J. Q.; Rockel, H.; Rumi, M.; Wu, X. L.; Marder, S. R.; Perry, J. W. *Nature* **1999**, *398*, 51. (b) Belfield, K. D.; Ren, X. B.; Van Stryland, E. W.; Hagan, D. J.; Dubikovsky, V.; Miesak, E. J. *J. Am. Chem. Soc*. **2000**, *122*, 1217.

(6) Liu, X.-J.; Feng, J.-K; Ren, A.-M.; Zhou, X. *Chem. Phys. Lett*. **2003**, *373*, 197.

(7) Das, S.; Nag, A.; Goswami, D.; Bharadwaj, P. K. *J. Am. Chem. Soc*. **2006**, *128*, 402–403.

(8) Abbotto, A.; Beverina, L.; Bozio, R.; Facchetti, A.; Ferrante, C.; Pagani, G. A.; Pedron, D.; Signorini, R. *Org. Lett*. **2002**, *4*, 1495.

(9) Wei, P.; Bi, X.; Wu, Z. *Org. Lett*. **2005**, *7*, 3199.

(10) (a) Yang, W. J.; Kim, D. Y.; Jeong, M.-Y.; Kim, H. M.; Jeon, S.-J.; Cho, B. R. *Chem. Commun*. **2003**, 2618. (b) Yang, W. J.; Kim, C. H.; Jeong, M.-Y.; Lee, S. K.; Piao, M. J.; Jeon, S.-J.; Cho, B. R. *Chem. Mater*. **2004**, *16*, 2783. (c) Lee, S. K.; Yang, W. S.; Choi, J. J.; Kim, C. H.; Jeon, S. J.; Cho, B. R. *Org. Lett*. **2005**, *7*, 323.

Published on Web 03/19/2010

past, metal-organic compounds have also been examined in search of high TPA activity as a change of the design paradigm.[11]

In the case of metal-organic compounds or coordination complexes, ligand design plays a crucial role. To obtain favorable properties, organic ligands have to be designed in such a way that they possess at least one of the following conjugated structural motifs:[12] donor-π-bridge-acceptor (D-π-A), donor-π-bridge-donor (D-π-D), acceptor-π-bridge-donor-π-bridge-acceptor (A-π-D-π-A), or donor-π-bridge-acceptor-π-bridge-donor (D-π-A-π-D). Metal binding appears to modulate the electron delocalization in these systems that can modify the value of the TPA cross section.[12] For example, it has been reported that in certain Schiff bases the third order non-linear optical (NLO) response is strongly accentuated upon binding to metal ions.[7] In these systems, coordination to the metal ion appears to introduce an electron acceptor property at the coordinating imino sites causing strong polarization. We were interested in examining if this concept can as well be extended to multisite coordination ligands. We have been working on the design and applications of phosphorus-supported hydrazone ligands for some time now.[13] Using these ligands we were able to assemble homo- and heterometallic derivatives that have interesting properties.[13] Recently, for example, we were able to prepare a new family of 3d-4f assemblies some of which were found to be single molecule magnets.[14] Spurred by this we decided to investigate if we can design appropriate ligands that either by themselves or upon metalation would exhibit non-linear optical properties.

To realize the above objectives, we prepared a novel phosphorus-supported multi dentate ligand P(*S*)[N(Me)N=CH-C_6H_3-*2*-OH-*4*-$N(CH_2CH_3)_2]_3$ (**1**) which can bind metal ions through imino and phenolate coordinating units. We anticipated that the formation of metal complexes would lead to a reduction of electron density at the coordinating sites. However, since the electron-releasing diethylamino group is in conjugation with the CH=N coordination unit, a strong electron delocalization is expected *after* coordination to metal ions. Electron polarization in such complexes might be anticipated to lead to non-linear optical properties. Accordingly, **1** has been used to prepare mononuclear complexes LM [M = Fe (**2**) Co (**3**)] as well as trinuclear complexes L_2M_3 [M = Mn (**4**), Ni (**5**), Zn (**6**), Mg (**7**), Cd (**8**)]. The synthesis, structure, absorption, and emission behavior and NLO properties of these compounds are reported in this paper.

Experimental Section

Reagents and General Procedures. Solvents and other general reagents used in this work were purified according to the standard procedures.[15] (*S*)PCl_3 (Fluka, Switzerland) and 4-(*N,N*-diethylamino)salicylaldehyde (Sigma Aldrich, U.S.A.) were used as purchased. $Mn(OAc)_2\cdot 4H_2O$, $Co(OAc)_2\cdot 4H_2O$, $Ni(OAc)_2\cdot 4H_2O$, $Zn(OAc)_2\cdot 2H_2O$, $Cd(NO_3)_2\cdot 4H_2O$, $MgCl_2$, $Fe(acac)_3$, and $Co(acac)_3$ were obtained from SD Fine Chemicals, Mumbai, India. (*S*)$P[N(Me)NH_2]_3$ was synthesized by a known procedure.[13a] *N*-Methylhydrazine was obtained as a gift from the Vikram Sarabhai Space Research Centre, Thiruvananthapuram, India and has been used as such.

Instrumentation. Electronic spectra were recorded on a Perkin-Elmer-Lambda-20 UV−vis spectrometer and on a Shimadzu UV-160 spectrometer, and fluorescence spectra were recorded at 25 ± 0.1 °C on a Varian Luminescence Cary spectrometer equipped with a 10 mm quartz cell using dichloromethane as the solvent. Electrospray ionization-high resolution mass spectra (ESI-HRMS) were recorded on a MICROMASS QUATTROII triple quadrupole mass spectrometer. The ESI capillary was set at 3.5 kV, and the cone voltage was 40 V. IR spectra were recorded as KBr pellets on a Bruker Vector-22 FTIR spectrophotometer operating from 400 to 4000 cm^{-1}. Elemental analyses of the compounds were obtained from Thermoquest CE instrument CHNSO EA/110 model. All the compounds were thoroughly evacuated (10^{-1} Torr) at 40 °C for 24 h before carrying out the elemental anlysis. ^1H and $^{31}P\{^1H\}$ NMR spectra were recorded in $CDCl_3$ solutions on a JEOL JNM LAMBDA 400 model spectrometer operating at 400.0 and 161.7 MHz respectively. Chemical shifts are reported in parts per million (ppm) with reference to internal tetramethylsilane (^1H) and external 85% H_3PO_4 (^{31}P).

X-ray Crystallography. Crystal data and other parameters for compounds **2**−**8** are given in Tables 1−2. Single crystals suitable for X-ray crystallographic analyses were obtained from a slow evaporation of a solution of dichloromethane-toluene mixture (**2**), dichloromethane-methanol mixture (**3**), chloroform-toluene mixture (**4**), dichloromethane-methanol-toluene mixture (**6**), chloroform−methanol mixture (**7**), and by slow diffusion of *n*-hexane into the dichloromethane/methanol mixture (**5**), dichloromethane-toluene mixture (**8**). The crystal data for all the compounds have been collected on a Bruker SMART CCD diffractometer using a Mo Kα sealed tube.

(11) (a) Verbiest, T.; Houbrechts, S.; Kauranen, M.; Clays, K.; Persoons, A. *J. Mater. Chem.* **1997**, *7*, 2175. (b) Whittall, I. R.; McDonagh, A. M.; Humphrey, M. G.; Samoc, M. *Adv. Organomet. Chem.* **1998**, *42*, 291. (c) McDonagh, A. M.; Humphrey, M. G.; Samoc, M.; Luther-Davies, B. *Organometallics* **1999**, *18*, 5195. (d) Whittall, I. R.; McDonagh, A. M.; Humphrey, M. G.; Samoc, M. *Adv. Organomet. Chem.* **1999**, *43*, 349. (e) Weyland, T.; Ledoux, I.; Brasselet, S.; Zyss, J.; Lapinte, C. *Organometallics* **2000**, *19*, 5235. (f) Hurst, S. K.; Humphrey, M. G.; Isoshima, T.; Wostyn, K.; Asselberghs, I.; Clays, K.; Persoons, A.; Samoc, M.; Luther-Davies, B. *Organometallics* **2002**, *21*, 2024. (g) Briñas, R. P.; Troxler, T.; Hochstrasser, R. M.; Vinogradov, S. A. *J. Am. Chem. Soc.* **2005**, *127*, 11851. (h) Zheng, Q.; He, G. S.; Prasad, P. N. *J. Mater. Chem.* **2005**, *15*, 579. (i) Zhang, M.-L.; Tian, Y.-P.; Zhang, X.-J.; Wu, J.-Y.; Zhang, S.-Y.; Wang, D.; Jiang, M.-H.; Chantrapromm, S.; Fun, H.-K. *Transition Met. Chem.* **2004**, *29*, 596–602. (j) Samoc, M.; Morrall, J. P.; Dalton, G. T.; Cifuentes, M. P.; Humphrey, M. G. *Angew. Chem., Int. Ed.* **2007**, *46*, 731–733. (k) Feuvrie, C.; Maury, O.; Bozec, H. L.; Ledoux, I.; Morrall, J. P.; Dalton, G. T.; Samoc, M.; Humphrey, M. G. *J. Phys. Chem. A* **2007**, *111*, 8980–8985. (l) Dragonetti, C.; Balordi, M.; Colombo, A.; Roberto, D.; Ugo, R.; Fortunati, I.; Garbin, E.; Ferrante, C.; Bozio, R.; Abbotto, A.; Bozec, H. L. *Chem. Phys. Lett.* **2009**, *475*, 245–249.

(12) (a) Das, S.; Nag, A.; Sadhu, K. K.; Goswami, D.; Bharadwaj, P. K. *J. Organomet. Chem.* **2007**, *692*, 4969. (b) Jana, A.; De, A. K.; Nag, A.; Goswami, D.; Bharadwaj, P. K. *J. Organomet. Chem.* **2008**, *693*, 1186–1194. (c) Jana, A.; Jang, S. Y.; Shin, J.-Y.; De, A. K.; Goswami, D.; Kim, D.; Bharadwaj, P. K. *Chem.—Eur. J.* **2008**, *14*, 10628–10638.

(13) (a) Chandrasekhar, V.; Azhakar, R.; Andavan, G. T. S.; Krishnan, V.; Zacchini, S.; Bickley, J.; Steiner, A.; Butcher, R. J.; Kögerler, P. *Inorg. Chem.* **2003**, *42*, 5989. (b) Chandrasekhar, V.; Azhakar, R.; Zacchini, S.; Bickley, J.; Steiner, A. *Inorg. Chem.* **2005**, *44*, 4608. (c) Chandrasekhar, V.; Azhakar, R.; Bickley, J.; Steiner, A. *Chem. Commun.* **2005**, 459. (d) Chandrasekhar, V.; Azhakar, R.; Pandian, B. M.; Bickley, J.; Steiner, A. *Eur. J. Inorg. Chem.* **2008**, *7*, 1116. (e) Chandrasekhar, V.; Pandian, B. M. *Acc. Chem. Res.* **2009**, *42*(8), 1047–1062.

(14) (a) Chandrasekhar, V.; Pandian, B. M.; Azhakar, R.; Vittal, J. J.; Clérac, R. *Inorg. Chem.* **2007**, *46*, 5140. (b) Chandrasekhar, V.; Pandian, B. M.; Boomishankar, R.; Steiner, A.; Vittal, J. J.; Houri, A.; Clérac, R. *Inorg. Chem.* **2008**, *47*, 4918.

(15) Furniss, B. S.; Hannaford, A. J.; Smith, P. W. G.; Tatchell, A. R. *Vogel's Text Book of Practical Organic Chemistry*, 5th ed.; ELBS, Longman: London, 1989.

(16) (a) *SMART & SAINT Software Reference manuals*, version 6.45; Bruker Analytical X-ray Systems, Inc.: Madison, WI, 2003. (b) Sheldrick, G. M. *SADABS a software for empirical absorption correction*, Version 2.05; University of Göttingen: Göttingen, Germany, 2002. (c) *SHELXTL Reference Manual*, version 6.1; Bruker Analytical X-ray Systems, Inc.: Madison, WI, 2000. (d) Sheldrick, G. M. *SHELXTL*, v.6.12; Bruker AXS Inc.: Madison, WI, 2001. (e) Sheldrick, G. M. *SHELXL97, Program for Crystal Structure Refinement*; University of Göttingen: Göttingen, Germany, 1997.

Table 1. Crystallographic Parameters for **2**–**5**

	2	**3**	**4**	**5**
empirical formula	$C_{36}H_{55}N_9O_5PSFe$	$C_{36}H_{51}CoN_9O_3PS$	$C_{86}H_{118}Mn_3N_{18}O_6P_2S_2$	$C_{151}H_{218}Cl_{14}Ni_6N_{36}O_{12}P_4S_4$
formula weight	812.77	779.82	1790.86	3830.29
temperature (K)	100(2)	100(2)	100(2)	100(2)
wavelength (Mo Kα))	0.71073 Å	0.71073 Å	0.71073 Å	0.71073 Å
crystal system	trigonal	triclinic	triclinic	monoclinic
space group	$P\bar{3}c1$	$P\bar{1}$	$P\bar{1}$	$P2(1)/n$
Unit cell dimensions				
a	12.073(5) Å	11.780(2) Å	12.533(3) Å	17.3154(8) Å
b	12.073(5) Å	13.638(3) Å	13.656(3) Å	23.5940(10) Å
c	32.033(5) Å	13.901(3) Å	14.790(3) Å	21.7367(10) Å
α	90°	97.13(3)°	67.226(4)°	90°
β	90°	93.09(3)°	73.680(4)°	96.4330(10)°
γ	120°	93.36(3)°	71.295(4)°	90°
volume	4044(2) $Å^3$	2208.0(8) $Å^3$	2174.9(8) $Å^3$	8824.4(7) $Å^3$
Z, density (calculated)	4, 1.335 g/cm^3	2, 1.173 g/cm^3	1, 1.367 g/cm^3	2, 1.442 g/cm^3
absorption coefficient	0.516 mm^{-1}	0.514 mm^{-1}	0.577 mm^{-1}	0.989 mm^{-1}
F (000)	1724	824	945	4004
crystal size(mm^3)	0.12 × 0.11 × 0.08	0.16 × 0.14 × 0.12	0.12 × 0.11 × 0.10	0.08 × 0.05 × 0.03
θ range for data collection	2.33 to 22.49°	2.21 to 26.00°	2.10 to 26.00°	1.97 to 26.00°
limiting indices	$-12 \le h \le 12$, $-12 \le k \le 12$, $-34 \le l \le 22$	$-14 \le h \le 13$, $-16 \le k \le 7$, $-17 \le l \le 16$	$-15 \le h \le 15$, $-16 \le k \le 15$, $-18 \le l \le 11$	$-21 \le h \le 21$, $-29 \le k \le 16$, $-26 \le l \le 25$
reflections collected	11230	12564	12351	49463
independent reflections	1655 [*R*(int) = 0.0944]	8502 [*R*(int) = 0.0384]	8369 [*R*(int) = 0.0481]	17316 [*R*(int) = 0.0652]
completeness to *θ* (%)	93.5	97.8	97.9	99.8
data/ restraints/ parameters	6257/0/430	8502/0/469	8369/0/539	17316/0/1022
Goodness-of-fit on F^2	1.158	0.973	1.004	1.020
final *R* indices [$I > 2\sigma(I)$]	R1 = 0.1766 wR2 = 0.4215	R1 = 0.0627 wR2 = 0.1421	R1 = 0.0722 wR2 = 0.1705	R1 = 0.0669 wR2 = 0.1649
R indices (all data)	R1 = 0.1881 wR2 = 0.4259	R1 = 0.0867 wR2 = 0.1560	R1 = 0.1125 wR2 = 0.2058	R1 = 0.1189 wR2 = 0.1986
largest diff. peak and hole (e $Å^{-3}$)	1.118 and −1.732	0.500 and −0.337	1.009 and −0.505	1.413 and −1.589

Table 2. Crystallographic Parameters for **6**–**8**

	6	**7**	**8**
empirical formula	$C_{173}H_{217}Zn_6N_{36}O_{12}P_4S_2Cl_2$	$C_{74}H_{110}Mg_3N_{18}O_8P_2S_2$	$C_{73}H_{104}Cd_3N_{18}O_6P_2S_2Cl_2$
formula weight	3708.07	1578.79	1863.90
temperature (K)	100(2)	100(2)	100(2)
wavelength (Mo Kα)	0.71073 Å	0.71073 Å	0.71073 Å
crystal system	monoclinic	triclinic	triclinic
space group	$C2/c$	$P\bar{1}$	$P\bar{1}$
unit cell dimensions			
a	14.792(5) Å	14.1599(12) Å	15.868(5) Å
b	26.013(9) Å	16.2110(14) Å	16.139(5) Å
c	48.219(5) Å	17.9945(15) Å	26.301(5) Å
α	90°	88.046(2)°	90.745(5)°
β	97.584(5)°	86.413(2)°	98.788(5)°
γ	90°	77.602(2)°	96.555(5)°
volume	18392(9) $Å^3$	4025.4(6) $Å^3$	4097(2) $Å^3$
Z, density (calculated)	4, 1.339 g/cm^3	2, 1.303 g/cm^3	2, 1.511 g/cm^3
absorption coefficient	0.946 mm^{-1}	0.194 mm^{-1}	0.988 mm^{-1}
F (000)	7764	1684	1912
crystal size (mm^3)	0.20 × 0.18 × 0.14	0.14 × 0.12 × 0.10	0.09 × 0.08 × 0.07
θ range for data collection	2.16 to 25.50°	2.14 to 26.00°	2.17 to 26.00°
limiting indices	$-17 \le h \le 17$, $-31 \le k \le 24$, $-57 \le l \le 58$	$-9 \le h \le 17$, $-15 \le k \le 19$, $-22 \le l \le 21$	$-18 \le h \le 19$, $-19 \le k \le 17$, $-19 \le l \le 20$
reflections collected	49507	22901	23049
independent reflections	17103 [*R*(int) = 0.0595]	15515 [*R*(int) = 0.0381]	15739 [*R*(int) = 0.0306]
completeness to *θ* (%)	99.9	98.0	97.8
data/ restraints/ parameters	17103/0/1100	15515/1/984	15739/0/976
GoF on F^2	1.023	1.031	1.026
final *R* indices [$I > 2\sigma(I)$]	R1 = 0.0572 wR2 = 0.1409	R1 = 0.0766 wR2 = 0.1950	R1 = 0.0612; wR2 = 0.1527
R indices (all data)	R1 = 0.0895 wR2 = 0.1638	R1 = 0.1193 wR2 = 0.2440	R1 = 0.0915 wR2 = 0.1856
largest diff. peak and hole (e $Å^{-3}$)	1.172 and −0.439	0.818 and −0.591	1.673 and −0.675

The program SMART[16a] was used for collecting frames of data, indexing reflections, and determining lattice parameters, SAINT[16a] for integration of the intensity of reflections and scaling, SADABS[16b] for absorption correction, and SHELXTL[16c,d] for space group and structure determination and least-squares refinements on F^2. All structures were solved by

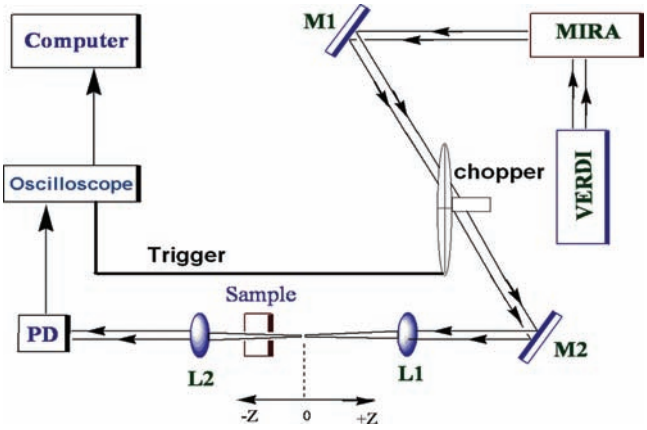

Figure 1. Experimental setup for *z*-scan measurement.

direct methods using the programs SHELXS-97[16e] and refined by full-matrix least-squares methods against F^2 with SHELXL-97.[16e] Hydrogen atoms were fixed at calculated positions, and their positions were refined by a riding model. All non-hydrogen atoms were refined with anisotropic displacement parameters. The disordered solvent molecules were refined isotropically. The crystal data for **2** was very poor. However, it can be used for confirming the molecular structure. Because of the poor quality of data, we did not attempt to discuss the bond parameters of this compound.

Experimental Setup for *Z*-Scan Measurements. TPA cross-section values of the samples have been measured by the open aperture *z*-scan (intensity scan) method.[17] Our femtosecond experimental setup (Figure 1) involves a mode-locked Coherent Mira Ti:Sapphire laser (Model 900) which is pumped by a Coherent Verdi frequency doubled Nd:Vanadate laser.

The model 900 Mira is tunable from 730 to 900 nm, and its repetition rate is 76 MHz. We employ blanking in our nonlinear transmission measurements by using a mechanical chopper MC1000A from Thorlabs at 50% duty cycle. The optimization of the frequency of the chopper was performed by eliminating the cumulative thermal effect arising from the sample heating with HRR pulses at excitation wavelength.[18] Liquid samples are held in a 1 mm path length quartz cuvette for the OA *z*-scan experiments. Using a 20 cm focal length lens, the 120 fs pulses are focused into the sample cell, which resulted in ~1 GW/cm^2 intensity at the focus. The 1 mm long sample cell satisfies the condition that the cell-length is less than the Rayleigh range of the focusing lens. Rayleigh range in our set up was 1.2 mm at 770 nm, as the beam waist at the focus was 17 μm. We scanned the sample through the focal point of the lens using a motorized translation stage (Newport Inc. model ESP 300), which has a minimum step size of 0.1 μm. This allows for a smooth intensity scan of the sample.

The transmitted beam through the sample is focused with a 7.5 cm focal length lens into a UV-enhanced amplified silicon photodiode detector (Thorlabs DET210). The peak-to-peak values from the photodiode are measured with an oscilloscope (Model Tektronix TDS 224, digital real time oscilloscope), which is triggered by the chopper frequency. The delay stage and the oscilloscope are interfaced with the computer using a GPIB card (National Instruments Inc.), and the data is acquired using LabVIEW programming. After acquiring the data, the results were fitted with the following equation:[18]

$$T(z) = 1 - \frac{\beta I_0 L}{2\sqrt{2}\left(1 + \left(\frac{Z}{Z_0}\right)^2\right)} \quad (1)$$

At different z positions, T is calculated and as all the other parameters are known, β can be calculated easily. Subsequent to obtaining the values of β, the TPA cross-section of the chromophore (σ_2, in units of 1 GM = 10^{-50} cm^4 s/(photon molecule) is generated from the expression: $\sigma_2 = \beta h\nu \times 10^3/Nc$, where ν is the frequency of the incident laser beam, N is Avogadro constant, c is the concentration of the chromophore in respective solvents. We take the known value of σ_2 for Rhodamine-6G in MeOH at 806 nm as the reference[19] for calibrating our measurement technique.

Syntheses. P(*S*)[N(Me)N=CH-C$_6$H$_3$-2-OH-4-N(CH$_2$CH$_3$)$_2$]$_3$ (LH$_3$, 1). To a stirred solution of P(*S*)[N(Me)NH$_2$]$_3$ (0.70 g, 3.5 mmol) in ethanol (60 mL) was added dropwise a solution of 4-(*N,N*-diethylamino)salicylaldehyde (2.04 g, 10.6 mmol) also in ethanol (60 mL) at room temperature. After the addition was over, the reaction mixture was stirred for 10 h. A yellowish brown solid that was formed was filtered and purified by recrystallization from dichloromethane/*n*-hexane (1:1) at room temperature. Yield: 2.20 g, 86%. Mp: 96 °C. UV−vis. (CH$_2$Cl$_2$) $\lambda_{max/nm}$ (ε/dm^3 mol^{-1} cm^{-1}): 352 (2.53 × 10^5), 230 (1.95 × 10^5), FT-IR (ν /cm^{-1}): 1638 (C=N). ^{1}H NMR (CDCl$_3$, δ, ppm): 1.14 (t, 18H, -N(CH$_2$CH$_3$)$_2$, ^3J(H−H) = 6 Hz); 3.26−3.35 (m, 21H, -N(CH$_3$) and -N(CH$_2$-CH$_3$)$_2$); 6.13−6.20 (m, 6H, aromatic), 6.99−7.01(m, 3H, aromatic), 7.72 (s, 3H imino), 10.97 (s, 3H, hydroxyl). ^{31}P NMR (CDCl$_3$, δ, ppm): 72.70 (s). ESI-MS (*m*/*z*): 725 (M$^+$). Anal. Calcd for C$_{36}$H$_{54}$N$_9$O$_3$PS: C, 59.73; H, 7.52; N, 17.41. Found: C, 59.66; H, 7.46; N, 17.32.

Preparation of Mononuclear Complexes (2)−(3). (*S*)P[N(Me)-N=CH-C$_6$H$_3$-2-O-4-N(C$_2$H$_5$)$_2$]$_3$Fe (2). To a solution of ligand (0.11 g, 0.15 mmol) in chloroform/methanol (30:30 mL) mixture, iron(III) acetylacetonate (0.06 g, 0.2 mmol) and triethylamine (0.3 mL) were added and allowed to stir for 6 h. Then this reaction mixture was filtered and evaporated to dryness. The product obtained was purified by crystallization as described in the X-ray crystallography section. Yield: 0.09 g, 76.2%. Mp: > 280 °C (d). UV−vis. (CH$_2$Cl$_2$) $\lambda_{max/nm}$ (ε/dm^3 mol^{-1} cm^{-1}): 376 (sh, 1.31 × 10^5), 350 (1.58 × 10^5), 280 (sh, 0.89 × 10^5), 237 (1.80 × 10^5). FT-IR (ν/cm^{-1}): 1606 (C=N). ESI-MS (*m*/*z*): 1191(M$^+$). μ_{eff} (300 K) 5.8 μ_B Anal. Calcd for C$_{36}$H$_{51}$N$_9$PO$_3$SFe: C, 55.67; H, 6.62; N, 16.23. Found: C, 55.62; H, 6.56; N, 16.21.

(*S*)P[N(Me)N=CH-C$_6$H$_3$-2-O-4-N(C$_2$H$_5$)$_2$]$_3$Co (3). To a solution of ligand (0.10 g, 0.14 mmol) in chloroform/methanol (30:30 mL), coblat(III) acetylacetonate (0.05 g, 0.14 mmol) and sodium acetate(0.07 g, 0.09 mmol) were added and allowed to stir for 6 h. Then this reaction mixture was filtered and evaporated to dryness to obtain **3**.

The same compound was also prepared by the treatment of Co(OAc)$_2$·4H$_2$O with ligand. The product obtained was purified by crystallization. Yield: 0.09 g, 84.0%. Mp: > 280 °C. UV−vis. (CH$_2$Cl$_2$) $\lambda_{max/nm}$ (ε/dm^3 mol^{-1} cm^{-1}): 364 (0.84 × 10^5), 290 (0.59 × 10^5) 254 (0.77 × 10^5). FT-IR (ν/cm^{-1}): 1609 (C=N). ^{31}P NMR (CDCl$_3$, δ, ppm): 79.8 (s). ESI-MS (*m*/*z*): 780.29 (M+H)$^+$. Anal. Calcd for C$_{36}$H$_{51}$N$_9$PO$_3$SCo: C, 55.36; H, 6.72; N, 16.15. Found: C, 55.26; H, 6.68; N, 16.06.

Preparation of Trinuclear Complexes (4−8). A general procedure was applied for the preparation of these metal complexes (**4**−**8**). The ligand (0.10 g, 0.14 mmol) was taken in the mixture of chloroform/methanol (30:30 mL), and triethylamine (0.2 mL)

(17) Sheik-Bahae, M.; Said, A. A.; Wei, T.; Hagan, D. J.; Van Stryland, E. W. *IEEE J. Quantum Electron.* **1990**, *26*, 760.
(18) Nag, A.; De, A. K.; Goswami, D. *J. Phys. B: At. Mol. Opt. Phys.* **2009**, *42*, 065103.
(19) (a) Sengupta, P.; Balaji, J.; Banerjee, S.; Philip, R.; Ravindra Kumar, G.; Maiti, S. *J. Chem. Phys.* **2000**, *112*, 9201. (b) Tian, P.; Warren, W. S. *Opt. Lett.* **2002**, *27*, 1634.

was added to this solution and stirred for 30 min. Corresponding metal salts (0.21 mmol) $Mn(OAc)_2 \cdot 4H_2O$, $Ni(OAc)_2 \cdot 4H_2O$, $Zn(OAc)_2 \cdot 2H_2O$, $Cd(NO_3)_2 \cdot 4H_2O$, or $MgCl_2$ were added to the above solution at room temperature and stirred for 6 h. The reaction mixture was filtered, and the filtrate was evaporated in vacuo to give the metal complexes. These were purified by crystallization as described in the X-ray crystallography section. The characterization data for these complexes are given below.

{(*S*)P[N(Me)N=CH-C_6H_3-2-O-4-N(C_2H_5)$_2$]$_3$}$_2$$Mn_3$ (4). Yield: 0.07 g, 63.1%. Mp: > 280 °C. UV−vis. (CH_2Cl_2) $\lambda_{max/nm}$ (ε/dm^3 mol^{-1} cm^{-1}): 363 (4.32×10^5) 348 (0.15×10^5), 242 (0.20×10^5). FT-IR (ν/cm^{-1}): 1607 (C=N). ESI-MS (*m*/*z*): 1606.53 $(M+H)^+$. Anal. Calcd for $C_{72}H_{102}N_{18}P_2O_6S_2Mn_3$: C, 53.81; H, 6.40; N, 15.70. Found: C, 53.78; H, 6.43; N, 15.63.

{(*S*)P[N(Me)N=CH-C_6H_3-2-O-4-N(C_2H_5)$_2$]$_3$}$_2$$Ni_3$ (5). Yield: 0.09 g, 76.9%. Mp: > 280 °C. UV−vis. (CH_2Cl_2) $\lambda_{max/nm}$ (ε/dm^3 mol^{-1} cm^{-1}): 397 (1.43×10^5), 346 (2.87×10^5), 283 (1.05×10^5), 238 (2.23×10^5). FT-IR (ν/cm^{-1}): 1607 (C=N). ESI-MS (*m*/*z*): 1617.53 $(M+H)^+$. Anal. Calcd for $C_{72}H_{102}N_{18}P_2O_6S_2Ni_3$: C, 53.51; H, 6.37; N, 15.61. Found: C, 53.48; H, 6.28; N, 15.76.

{(*S*)P[N(Me)N=CH-C_6H_3-2-O-4-N(C_2H_5)$_2$]$_3$}$_2$$Zn_3$ (6). Yield: 0.09 g, 77.8%. Mp: > 280 °C. UV−vis. (CH_2Cl_2) $\lambda_{max/nm}$ (ε/dm^3 mol^{-1} cm^{-1}): 386 (2.14×10^5), 343 (4.16×10^5), 280 (1.43×10^5), 236 (3.14×10^5). FT-IR (ν/cm^{-1}): 1608 (C=N). ^{1}H NMR ($CDCl_3$, δ, ppm): 0.64 (t, 36H, -N(CH_2CH_3)$_2$, J(H−H) = 5.2 Hz); 2.84 (b, 24H, -N(CH_2CH_3)$_2$); 3.16 (d, 18H, -NCH_3, $^3J(^1H-^{31}P)$ = 8.8 Hz); 5.67 (d, 6H, aromatic, ^3J(H−H) = 4.8 Hz); 6.32 (s, 6H, aromatic); 6.57 (d, 6H, aromatic, ^3J(H−H) = 7.2 Hz); 8.04 (s, 6H, imino). ^{31}P NMR ($CDCl_3$, δ, ppm): 72.00 (s). ESI-MS (*m*/*z*): 1637.52 $(M+H)^+$. Anal. Calcd for $C_{72}H_{102}N_{18}P_2O_6S_2Ni_3$: C, 52.92; H, 6.29; N, 15.44. Found: C, 52.82; H, 6.35; N, 15.34.

{(*S*)P[N(Me)N=CH-C_6H_3-2-O-4-N(C_2H_5)$_2$]$_3$}$_2$$Mg_3$ (7). Yield: 0.08 g, 75.5%. Mp: > 280 °C. UV−vis. (CH_2Cl_2) $\lambda_{max/nm}$ (ε/dm^3 mol^{-1} cm^{-1}): 383 (1.93×10^5), 339 (4.45×10^5), 277 (0.93×10^5), 231 (2.23×10^5). FT-IR (ν/cm^{-1}): 1608 (C=N). ^{1}H NMR ($CDCl_3$, δ, ppm): 0.61 (t, 36H, -N(CH_2CH_3)$_2$, ^3J(H−H) = 5.2 Hz); 2.81 (b, 24H, -N(CH_2CH_3)$_2$); 3.12 (d, 18H, -NCH_3, J(H−H) = 8.8 Hz); 5.69 (d, 6H, aromatic, ^3J(H−H) = 6.8 Hz); 6.19 (s, 6H, aromatic); 6.62 (d, 6H, aromatic, ^3J(H−H) = 6.8 Hz); 8.07 (s, 6H imino). ^{31}P NMR ($CDCl_3$, δ, ppm): 70.04 (s). ESI-MS (*m*/*z*): 1515.67 $(M+H)^+$. Anal. Calcd for $C_{72}H_{102}N_{18}P_2O_6S_2Mg_3$: C, 57.12; H, 6.80; N, 16.66. Found: C, 57.10; H, 6.78; N, 16.68.

{(*S*)P[N(Me)N=CH-C_6H_3-2-O-4-N(C_2H_5)$_2$]$_3$}$_2$$Cd_3$ (8). Yield: 0.09 g, 73.5%. Mp: > 280 °C. UV−vis. (CH_2Cl_2) $\lambda_{max/nm}$ (ε/dm^3 mol^{-1} cm^{-1}): 351 (2.42×10^5), 245 (0.96×10^5), 229 (1.15×10^5). FT-IR (ν/cm^{-1}): 1606 (C=N). ^{1}H NMR ($CDCl_3$, δ, ppm): 0.70 (t, 36H, -N(CH_2CH_3)$_2$, ^3J(H−H) = 5.6 Hz); 2.78 (m, 24H, -N(CH_2CH_3)$_2$); 3.31 (d, 18H, -NCH_3, $^3J(^1H-^{31}P)$ = 9.2 Hz); 5.74 (d, 6H, aromatic, ^3J(H−H) = 7.2 Hz); 6.23 (s, 6H, aromatic); 6.64 (d, 6H, aromatic, ^3J(H−H) = 6.8 Hz); 7.80 (s, 6H imino). ^{31}P NMR ($CDCl_3$, δ, ppm): 72.48 (s). ESI-MS (*m*/*z*): 1780.66 $(M+H)^+$. Anal. Calcd. for $C_{72}H_{102}N_{18}P_2O_6S_2Cd_3$: C, 48.47; H, 5.77; N, 14.14. Found: C, 48.40; H, 5.74; N, 14.24.

Results and Discussion

Synthetic and Spectroscopic Aspects. Phosphorus(V) hydrazides have been used by Majoral and co-workers for the construction of macrocycles and cryptands,[20,21] while Katti and co-workers[22] have used them to prepare transition metal complexes. We have been interested in elaborating cyclic and acyclic phosphorus(V) hydrazides

Scheme 1. Synthesis of **1**

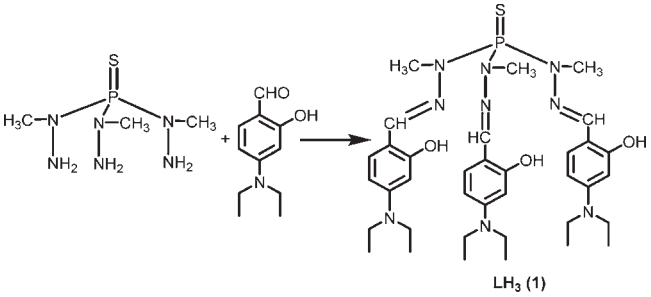

Scheme 2. Synthesis of Mononuclear Complexes (**2** and **3**)

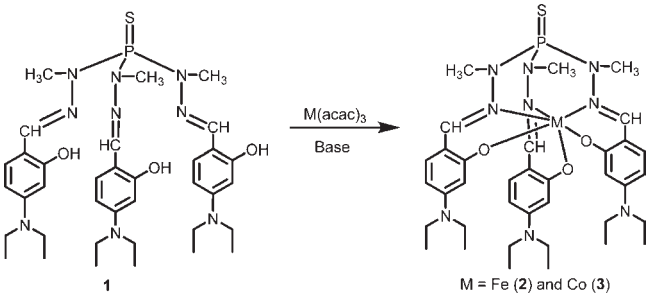

for a variety of purposes including assembling multidentate ligands. Some of these have been used to build homonuclear mono- or trimetallic complexes while some others have been used to prepare heteronuclear trimetallic 3d-4f complexes.[13] The latter possess interesting magnetic properties with some members displaying single-molecule-magnetism behavior. In light of this versatility we were interested in designing systems that would possess interesting NLO properties.[14] Accordingly, the ligand (*S*)P[N(Me)N=CH-C_6H_3-*2*-OH-*4*-N-(C_2H_5)$_2$]$_3$ (LH_3) (**1**) was prepared by the condensation of (*S*)P [N(Me)NH_2]$_3$ with *4*-(*N*, *N*-diethylamino) salicylaldehyde (Scheme 1). ^{31}P{^{1}H} NMR spectrum of **1** showed a single at 72.7 ppm. This may be compared with the chemical shift of the parent trihydrazide which occurs at 84.5 ppm. The upfield shifting of the chemical shift in the ^{31}P NMR, upon hydrazone formation, has been reported earlier.[13] The ligand LH_3 has three imino nitrogen and three phenolic oxygen atoms for coordination to the metal ion. Other than these coordinating groups, the ligand has three -NEt_2 groups at the *-meta* position relative to the phenolic group, as donors for electron delocalization. Reaction of LH_3 with trivalent metal salts [Co(acac)$_3$ and Fe(acac)$_3$] in the presence of a base leads to the formation of the neutral, mononuclear complexes LFe (**2**) and LCo (**3**) (Scheme 2). Also the reaction of the ligand with $Co(OAc)_2 \cdot 4H_2O$ leads to the formation of the mononuclear complex **3** by aerial oxidation of Co(II). On the other hand reaction of LH_3 with divalent metal salts $MX_2 \cdot nH_2O$ [M = Mn or Ni, X = OAc ; *n* = 4; M = Zn, X = OAc, *n* = 4; M = Mg, X = Cl, *n* = 0; M = Cd, X = NO_3, *n* = 4] affords the neutral, trinuclear complexes L_2M_3 **4**−**8** (Scheme 3).

All the diamagnetic complexes showed singlets in their ^{31}P{^{1}H} NMR: **3** (79.8), **6** (72.0 ppm), **7** (70.0 ppm), **8** (72.5 ppm); in contrast, as discussed above, the chemical shift of **1** is observed at 72.7 ppm. Further, all the

(20) Majoral, J. P.; Badri, M.; Caminade, A.-M.; Delmas, M.; Gaset, A. *Inorg. Chem.* **1988**, *27*, 3873.
(21) Mitjaville, J.; Caminade, A. M.; Majoral, J. P. *Chem. Commun.* **1994**, 2161.
(22) Katti, K. V.; Reddy, V. S.; Singh, P. R. *Chem. Soc. Rev.* **1995**, *24*, 97.

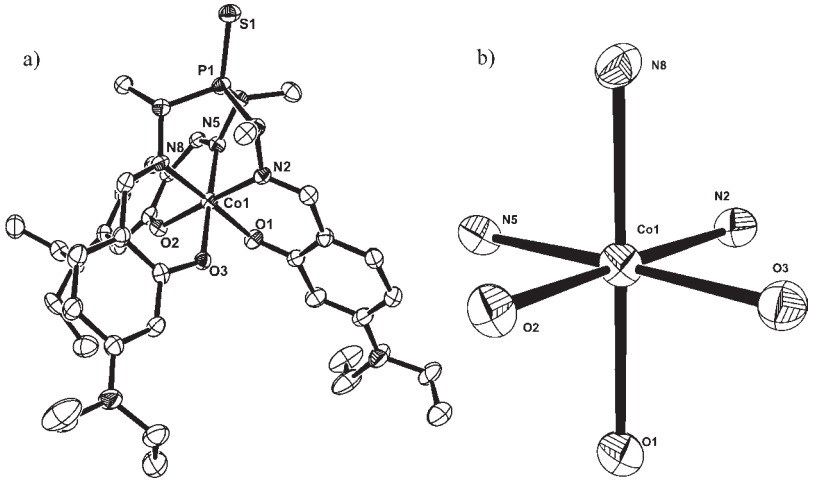

Figure 2. (a) ORTEP picture of **3**. Thermal ellipsoids are set at 50%. Hydrogen atoms and solvent molecules are omitted for clarity. (b) Coordination environment around Co in **3**.

Scheme 3. Synthesis of Trinuclear Complexes (**4**−**8**)

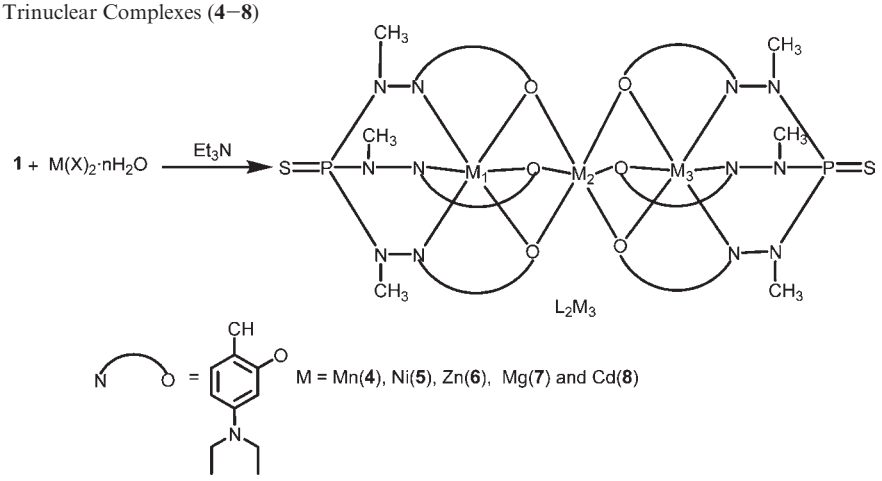

complexes showed $(M+H)^+$ peaks in their ESI-MS (see Experimental Section). FT-IR spectra of all the complexes shows peaks around 1607 cm^{-1} (C=N) which may be compared with that observed in the ligand at 1638 cm^{-1}.

X-ray Crystal Structures. The molecular structures of **2** and **3** are similar and were confirmed by X-ray crystallography (see Figure 2 for the molecular structure of **3**). As mentioned earlier in the Experimental Section, the X-ray data for the Fe(III) complex (**2**) is poor. Although this is useful for obtaining the molecular structure, the bond parameters are not accurate to merit discussion.

2 and **3** are both neutral, mononuclear complexes (LM) as a result of the perfect match between the deprotonated ligand L^{3-} and M^{3+}. The ligand encapsulates the metal ion by a concerted coordination action of all the three hydrazone arms. The resulting facial coordination mode around the metal ion results utilizes all the three imino nitrogen (3N) and the phenolate oxygen (3O) atoms. Selected metric parameters of **3** are given in Table 3. The other data are given in Supporting Information. The Co−N and Co−O bond distances in **3** are almost similar (Co−N_{avg} 1.912(3) and Co−O_{avg} 1.896(3) Å. These distances are shorter in comparison to those found in the trinuclear complexes **4**−**8** (see below).

Table 3. Selected Average Bond Distances (Å) and Bond Angles (deg) for **3**−**8**

compounds	M_t-O_{avg}	M_t-N_{avg}	M_c-O_{avg}	M_t-M_t	M_t-M_c-M_t
3[a]	1.896(3)	1.912(3)			
4[b]	2.131(3)	2.207(4)	2.202(3)	5.971(12)	180.00
5	2.046(4)	2.032(4)	2.065(3)	5.650(10)	177.50(3)
6	2.079(3)	2.117(3)	2.094(3)	5.740 (9)	179.50(2)
7	2.037(3)	2.166(4)	2.082(3)	5.624(2)	177.05(6)
8	2.222(4)	2.278(6)	2.321(4)	6.276(2)	180.00
	2.223(4)	2.265(5)	2.299(4)		180.00

[a] Only one type of metal ion is present. [b] M_t = terminal metal ions (labeled M_1 and M_3 in Scheme 3). M_c = central metal ion (labeled M_2 in Scheme 3).

The molecular structures of L_2Mn_3, L_2Ni_3, L_2Zn_3, L_2Mg_3, and L_2Cd_3 (**4**−**8**) are similar and were confirmed by X-ray crystallography. The unit cell of **8** contains two independent molecules. The molecular structure of **4** is shown in Figure 3, those of the others are given in Supporting Information. As shown by us earlier phosphorus-supported tris hydrazone ligands containing phenolate side chains *always* interact with divalent metal ions affording trinuclear complexes. In the current instance also two trianionic L^{3-} ligands interact with three divalent metal ions holding them together in a linear assembly. Each trianionic ligand coordinates in a tris chelating,

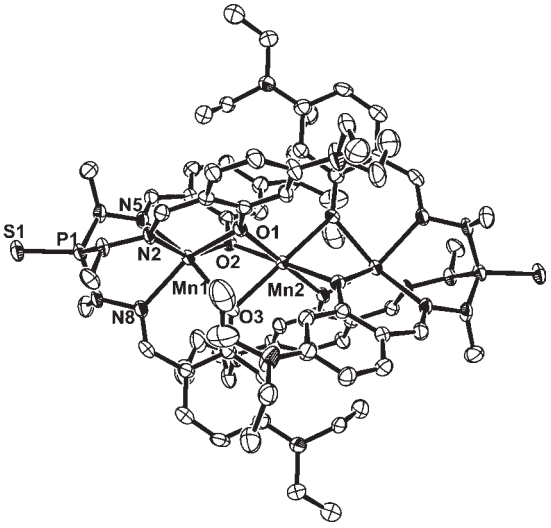

Figure 3. ORTEP picture of **4**. Thermal ellipsoids are set at 30%. Hydrogen atoms and solvent molecules are omitted for clarity.

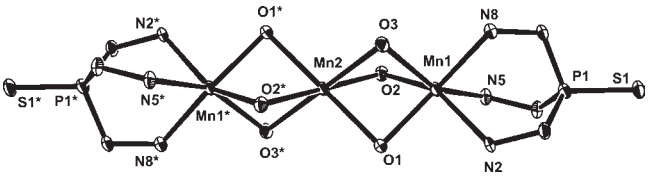

Figure 4. Core view of **4**. Thermal ellipsoids are set at 30%. Other atoms are omitted for clarity.

hexa-dentate manner and ligand provides three imino and three phenolate oxygen atoms for coordination to the metal ions. Among the three metal ions, the coordination environment around the two terminal metal ions is similar (3N, 3O) while the central metal ion has a 6O coordination environment (three O from each ligand) (Figures 3−4). All the three metal ions in the trinuclear assembly are present in a distorted octahedral geometry. In all the complexes the phenolate oxygen atoms act as bridging ligands and connect the terminal and central metal ions. As result of this phenolate bridge between the terminal and central metal ion, three four-membered $\overline{M_t\text{-}O\text{-}M_c\text{-}O}$ rings are formed. The coordination of imino nitrogen atoms to the terminal metal ions leads to the formation of three six-membered $\overline{P\text{-}N\text{-}N\text{-}M\text{-}N\text{-}N}$ rings resulting in a cryptand-type architecture (Figures 3−4). Further, the coordination of imino nitrogen and phenolate oxygen atoms leads to the formation of three more six-membered rings ($\overline{M\text{-}O\text{-}C\text{-}C\text{-}C\text{-}N}$). Interestingly, overall, the coordination of the ligand to the metal ions leads to the simultaneous formation of 18 rings in the trinuclear complex (Figure 4). Out of these, 12 are six-membered while 6 are four-membered. In all these compounds, the metal ions are arranged in an almost linear fashion. This leads to the formation of a paddle-wheel type of architecture when viewed through the intermetal axis (Figure 5). We have seen a similar architecture for other trimetallic complexes also.[12,13]

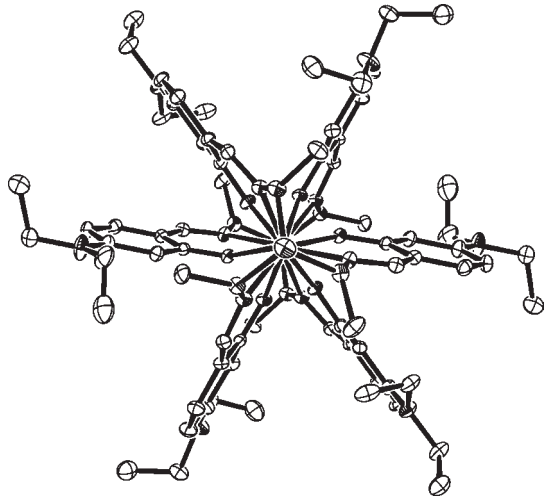

Figure 5. Paddle wheel view of **4** while viewed along inter metal axis. Thermal ellipsoids are set at 30%.

Selected average bond distance and angle data for complexes **4**−**8** are given in Table 3. Some of the important structural features observed in these complexes are as follows. In *all* the trinuclear complexes the M-O and M-N distances are longer than those observed in mononuclear complexes indicating a tighter binding in the latter in comparison to the former. In contrast to **3**, in **4**, **6**, **7**, and **8** the M_t-N bond distance is slightly longer than the M_t-O bond distance. In **5**, on the other hand, these two distances are similar. Among the M-O distances, in all the compounds, the M_c-O bond distance is slightly longer than M_t-O bond distance (Table 3). Although the M-O and M-N distances in **4**−**7** are similar, those observed in the trinuclear cadmium complex **8** are significantly longer because of the larger size of the Cd^{2+} in comparison with the other metal ions involved. This is also reflected in the distance between the two terminal metal ions(M_t-M_t). While this distance spans a narrow range between 5.624 to 5.971 Å in compounds **4**−**7**, in **8** this is substantially longer, 6.276(2) Å. Interestingly, although all the trinuclear complexes are linear, the inter metal angle (M_t-M_c-M_t) is a perfect 180° for **4** and **8** while for **3**, **5**, and **7** this value is slightly less (Table 3). Other bond parameters for **2**−**8** are provided in the Supporting Information.

Two-Photon Absorption Studies by *Z*-Scan Measurement. Before attempting the two-photon studies on **1**−**8**, the absorption and emission features of these compounds were examined. The optical spectroscopic data are summarized in Table 4. The absorption spectra of **1**−**8** in dichloromethane (1.0 μM) are characterized by peaks both at the high energy and low energy [cf. **1**, λ_{max} (nm) ($\varepsilon_{max} \times 10^4$/dm^3 mol^{-1} cm^{-1}); 230 (19.50), 352 (25.30)] (Figure 6). These spectra are typical for *N,N*-diethylamino-containing compounds, and the absorptions are due to intraligand $\pi-\pi^*$ transitions.[23] The absorption spectra of **1** and the trinuclear cadmium complex are nearly identical. The absorbance values of **4** at 1.0 μM concentration are very low. Another feature of complexes **2**−**7** is that new broad bands or shoulders are seen at ~280 nm and

(23) Chandrasekhar, V.; Bag, P.; Pandey, M. D. *Tetrahedron* **2009**, *65*, 9876–9883.

Table 4. Optical Absorption and Emission Data of **1**−**8**

compounds	absorbance (λ_{max}/nm) ($\varepsilon_{max} \times 10^4$/dm^3 mol^{-1} cm^{-1})	λ_{em}, nm	Φ_F
1	230 (19.50), 352 (25.30)	316, 333, 379	0.079
2	237 (18.01), 280 (sh 8.9), 350 (15.18), 376 (sh 13.1)	315, 415	0.042
3	254 (7.7), 290 (5.99), 364 (8.48)	329, 421	0.073
4	242 (2.04), 348 (1.50), 363 (43.28)	321, 435	0.066
5	238 (22.32), 283 (10.57), 346 (28.72), 397 (14.30)	318, 415	0.020
6	236 (31.41), 280 (14.3), 343 (41.67), 386 (21.42)	413, 416	0.013
7	231 (22.23), 277 (9.3), 339 (44.5), 383 (19.35)	314, 366, 406	0.040
8	229 (11.57), 245 (9.68), 351 (24.25)	316, 415	0.048

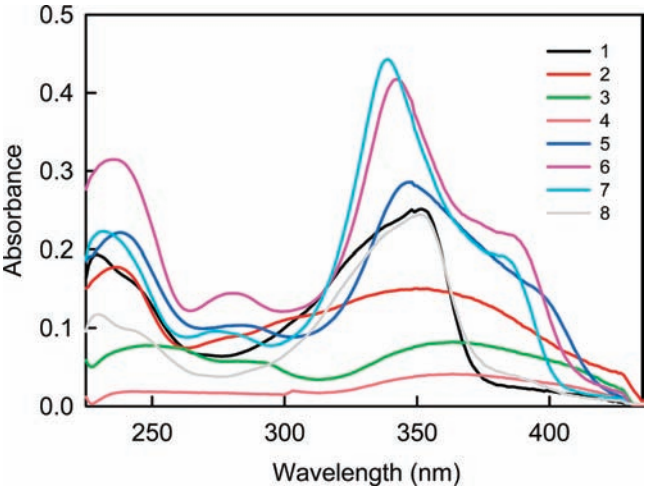

Figure 6. UV−vis spectra of **1**−**8** (1.0 μM) in dichloromethane solution.

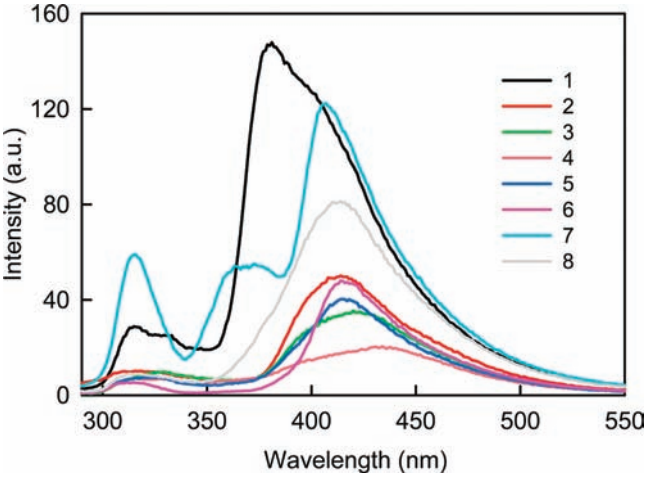

Figure 7. Fluorescence spectra of **1**−**8** (1.0 μM) in dichloromethane solution. The excitation wavelength was 280 nm.

~385 nm, probably arising because of metal-perturbed intraligand charge transfer (ILCT) transition.[24] Compound **1** shows an emission around 379 nm upon excitation at 280 nm. A few low energy bands are also seen in the emission spectra for this compound (Figure 7). The band at 379 nm was red-shifted upon metalation. However, **7** showed a new broadband at 366 nm (Figure 7). Fluorescence quantum yields in each case were determined by comparing the emission intensity of the sample with that of the quinine sulfate (quantum yield $\Phi = 0.54$ in 1N sulphuric acid).[24] Quantum yield of **1** was found to be 0.079 which further decreases upon metalation. It is possible that the partial charge transfer from the fluorophore to the metal ion might be responsible for the quenching of the fluorescence intensity. However, this proposal is tentative and needs to be confirmed by more detailed studies.

(24) (a) Ray, D.; Nag, A.; Goswami, D.; Bharadwaj, P. K. *J. Lumin.* **2009**, *129*, 256–262. (b) Meech, S. R.; Phillips, D. *J. Photochem.* **1983**, *23*, 193.

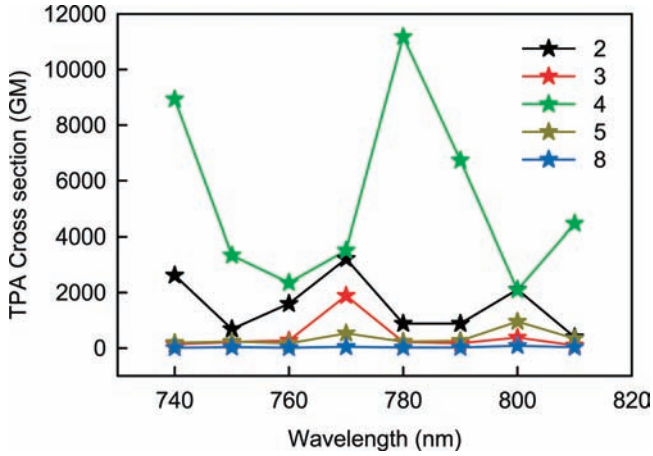

Figure 8. Two photon spectra of the entire complex in dichloromethane calculated using open aperture *z*-scan method.

Tris-hydrazone ligand (**1**) is a multisite coordination ligand where the imino and phenolic groups act as coordinating units. In addition, the ligand also contains electron-releasing diethylamino substituents which are attached to the aromatic phenyl groups. Complexation with transition metal ion results in an electron donation from coordinating units toward the metal ion. This results in a depletion of electron density at these coordinating units and probably causes them to become less electron donating. Since the electron−releasing diethylamino group is in conjugation with the CH=N unit, a strong delocalization is created in the ligand unit. As a result a third order non-linear response is seen after complexation. The non-linear optical measurements were performed in the near-infrared region since it is clear from the absorption spectra that ligand (**1**) and the metal complexes (**2**−**8**) are transparent in this region. The open-aperture *z*-scan traces for **2** and **4** are given in Figure 8 (for the others, see Supporting Information). The results of this study are summarized in Table 5.

The free ligand (**1**), Zn(II) (**6**) and the Mg(II) (**7**) complexes do not show any TPA activity. Among all other complexes, **2** and **4** are the ones with the highest TPA cross section values at all wavelength ranges studied. We observe a slight decrease in TPA value from Mn(II) to Fe(III) because of a decrease in ionic radius as well as a decrease in the number of ligands in the complexes from **4**

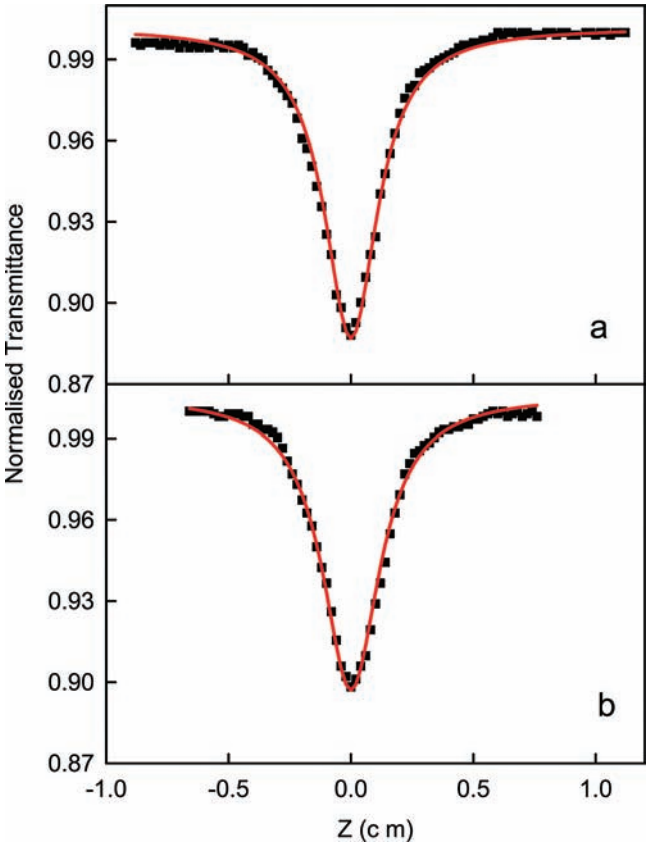

Figure 9. Open-aperture *z*-scan traces for **2** (a) and **4** (b). Solid lines are the best fitted of the experimental data.

Table 5. TPA Cross Section Values for the Complexes **2**−**5** and **8**

complex	concentration [10^{-3} mol L^{-1}]	2PA λ_{max} [nm]	σ_2 (GM) at peak	σ_2 (GM) at 770 nm
2	1	770	3213.3	3213.3
3	1	770	1889	1889.0
4	1	780	11177	3515.9
5	1	800	954	534.5
8	10	800	86.5	45.1

(contains two ligands) to **2** (contains one ligand), which possibly gives an extended delocalization of electrons in **4**. Lewis acidity[25] of the metal centers plays a key role in enhancement of TPA activity. This is due to an increase in the size of different metal centers having the same oxidation state.[25] In mononuclear complexes, a large decrease in TPA value is observed on going from **2** to **3** because of a small change in the Lewis acidity of the metal center of the complexes. In the trinuclear complexes, Lewis acidity decreases from Mn(II) to Ni(II) which is reflected in the TPA values of the respective complexes. TPA maxima positions for the complexes are red-shifted as we go from Mn(II) to Ni(II) to Cd(II). It is interesting to compare the TPA values obtained in the present instance with metal complexes known before. For example, a Zn(II) complex of a Schiff base has been shown to possess a TPA of 10736 GM at 890 nm.[7] However, the design principles of enhancing the TPA values in metal complexes are not fully clear.

We have also measured the TPA spectra of all complexes in the wavelength range 740−810 nm (Figure 8). The observed absorption maxima occur at 770 nm for complexes **2** and **3**, at 780 nm for complex **4**, and at 800 nm for complexes **5** and **8.** All the TPA spectra of these complexes follow similar trends as the single photon spectra of the respective complexes. This indicates that there is no major change in the excited state conformation as compared to the ground state conformation of the respective complexes during transition. Open-aperture *z*-scan traces for **2** and **4** are given in the Figure 9, while **3**, **5**, and **8** are given in the Supporting Information section.

Within the limitation of our experimental set up having a wavelength tuning range of 740−810 nm, we are unable to detect any two-photon induced fluorescence (TPIF) signal with reference to Rhodamine-6G for **1**−**8**. The absence of TPIF in **1**, **6**, and **7** is not surprising as they also do not show any measurable TPA. Metal mediated two-photon process has often been attributed to extended electron-delocalization due to the metal ion.[7] However, the observed single-photon fluorescence quenching with metalation of the ligand [**1**] might be the reason for the difficulty in observing the TPIF activity even for the samples with TPA under our experimental conditions. Limitation in the measurement of TPIF might also be attributed to the *two photon absorption excited intramolecular energy transfer process*, which essentially is the re-absorption of the emitted photon by the molecule itself.[26] This occurs when the TPIF energy coincides with the absorption energy.

Conclusion

We have utilized the tri-armed phosphorus hydrazide (*S*)P[N(Me)NH_2]$_3$ to assemble a phosphorus-supported ligand (*S*)P[N(Me)N=CH-C_6H_3-*2*-OH-*4*-N(CH_2CH_3)$_2$]$_3$ (**1**) for the study of two photon absorption process. This ligand forms both mono- and trinuclear complexes depending on the oxidation state of the metal ion used. Two-photon absorption studies reveal that the ligand does not have an NLO activity while some of its metal complexes possess NLO activity. Among the metal complexes, LFe (**2**) and L_2 Mn_3 (**4**) show high TPA cross section values.

Acknowledgment. We are thankful to the Department of Science and Technology (DST), New Delhi, for financial support including support for a CCD X-ray Diffractometer facility at IIT-Kanpur. B.M., T.S., and P.B. thank CSIR and S.K.M. thanks UGC India, respectively, for a Research Fellowship. V.C. is thankful to the DST for a J. C. Bose National fellowship.

Note Added after ASAP Publication. This paper was published on the Web on March 19, 2010. An additional author, Ramachandran Azhakar, was added to the paper. The corrected version was reposted on March 29, 2010.

Supporting Information Available: ORTEP diagrams of **2**, **5**, **6**, **7**, and **8**. Open-aperture *z*-scan traces for **3**, **5**, and **8**. Selected bond length and bond angle data for **2**−**8**. This material is available free of charge via the Internet at http://pubs.acs.org.

(25) Zhang, X. B.; Feng, J.-K.; Ren, A.-M. *J. Organomet. Chem.* **2007**, *692*, 3778.

(26) (a) He, G. S.; Lin, T.-C.; Cui, Y.; Prasad, P. N.; Brousmiche, D. W.; Serin, J. M.; Fréchet, J. M. J. *Opt. Lett.* **2003**, *28*, 768. (b) Oar, M. A.; Dichtel, W. R.; Serin, J. M.; Fréchet, J. M. J.; Rogers, J. E.; Slagle, J. E.; Fleitz, P. A.; Tan, L.-S.; Ohulchanskyy, T. Y.; Prasad, P. N. *Chem. Mater.* **2006**, *18*, 3682.